Ocean Dynamics (2019) 69:1023–1036
https://doi.org/10.1007/s10236-019-01298-8

Partial residence times: determining residence time composition in different subregions

Lei Lin [1,2] · Zhe Liu [2,3]

Received: 7 March 2019 / Accepted: 29 July 2019 / Published online: 10 August 2019

Abstract
Residence time (RT) is a diagnosis widely used to quantify the water exchange rate and mass transport timescale in semi-enclosed systems. The RT focuses on only the total time a water parcel spends in a system (i.e., control region). However, for a system that consists of several subregions (e.g., sub-bays or functional zones), the RT will not include information about the time spent in different subregions. To determine the RT compositions in different subregions, partial residence times (PRTs) are proposed and defined as the amount of time a water parcel spends in different subregions until leaving the control region. The equations for PRTs are derived using the adjoint method, which can quickly determine the variation of PRTs in time and space. To validate the PRT diagnostic equation and numerical model, a test is conducted in an idealized 1D channel with idealized tidal currents. The numerical results are in excellent agreement with the analytical solution. Finally, the PRT method is applied to tide-dominated Jiaozhou Bay. The PRTs in six functional subregions of Jiaozhou Bay are derived, and the detailed RT compositions of the different functional subregions are presented. The application indicates that PRTs could provide detailed information and new insights into the water exchange process.

Keywords Residence time · Water exchange · Transport timescale · Adjoint method · Jiaozhou Bay

1 Introduction

Coastal environmental problems (e.g., eutrophication, harmful algal blooms, and hypoxia) are usually closely related to the water exchange capacity of the marine system involved (e.g., Jickells 1998; Lucas et al. 2009; Lillebø et al. 2005). Several timescales have been proposed to quantify the water exchange capacity, such as the flushing time, turnover time, half-life time, age, and residence time (RT) (e.g., Bolin and Rodhe 1973; Deleersnijder et al. 2001; Prandle 1984; Monsen et al. 2002; Luff and Pohlmann 1995). Among these timescales, RT is one of the most widely used indicators. The RT was defined as the amount of time a water parcel (or particle) spends in a given control region before leaving (Bolin and Rodhe 1973; Takeoka 1984). According to the definition, RT could be used to quantify the water exchange rate of the control region. In addition, RT is appealing because this timescale can summarize the complete and complex dynamics of a system in a single figure that can easily be compared with other characteristic timescales to identify the most relevant processes (Delhez 2013). In the last two decades, the RT concept and resolution method have been well developed based on the constituted-oriented age and residence time theory (CART) (Deleersnijder et al. 2001; Delhez and Deleersnijder 2002; Delhez et al. 2004), and RT has been widely used in studies of marine hydrodynamics and ecology (e.g., Du and Shen 2016; Gong et al. 2008; Jeyar et al. 2017; Meyers et al. 2017; Ranjbar and Zaker 2017; Sun et al. 2014; Yuan et al. 2007).

Marine systems are commonly divided into several subregions according to the topography and shoreline features or the social demands and surrounding environment (Luan and Dong 2002). The water exchange and transport processes in these subregions of the control region are also of interest and concern (e.g., Gong et al. 2009; Liu et al. 2012b). The transport timescales in different subregions could be used to

Responsible Editor: Eric Deleersnijder

✉ Zhe Liu
zliu@ouc.edu.cn

[1] State Key Laboratory of Estuarine and Coastal Research, East China Normal University, Shanghai 200062, China

[2] Key Laboratory of Marine Environment and Ecology, Ministry of Education, Ocean University of China, 238 Songling Road, Qingdao 266100, China

[3] Present address: Department of Earth Sciences, National Natural Science Foundation of China, Beijing, China

quantify the local exchange capacity in these subregions and to compare differences in the transport rates between subregions. This can be used to build a quantitative understanding of the regional heterogeneity in hydrodynamics in one marine system; however, new timescale variables must be added. For example, based on the concept of "age," Mouchet et al. (2016) proposed the concept of "partial age" to quantify the amount of time a tracer parcel has spent in different subregions.

The RT can tell us the total amount of time that a water parcel or particle remains in the marine system of interest, but the RT cannot tell us the specific amount of time the parcel or particle spends in different subregions of the system. Thus, it is difficult to distinguish the influences of water or matter on different subregions using only one "RT" variable. The time a particle or water parcel spends in different subregions is important information to marine ecologists and managers for determining the length of time that nutrient-rich or pollutant water masses influence different subregions in a marine system, e.g., ecological preservation zones, agricultural zones, and algal bloom zones. This can be also important in understanding symptoms of environmental degradation in systems where overall water exchange levels are low, but where ecological values have deteriorated to below environmental management benchmarks in just part of the system (e.g. semi-enclosed embayment in Cockburn Sound, Australia, Fraser and Kendrick 2017; Olsen et al. 2018). Therefore, in addition to the RT, it is necessary to supplement new variables to determine the RT compositions in different subregions (subregional RT, hereafter) and quantify the duration of water mass subregional influences. De Brauwere et al. (2011) decomposed the Scheldt Estuary (Belgium, Netherlands) into 13 boxes and defined the "subdomain exposure time" to quantify the amount of time spent in different boxes. The "subdomain exposure time" indicates the subregional RT of the water masses averaged in one box. However, the remnant function method used by de Brauwere et al. (2011) could not derive the continuous spatial variability of the subregional timescales in the system due to the considerable computational cost (Delhez et al. 2004). In some cases, the high spatiotemporal variability of the subregional RT in a study zone is of interest, such as the difference in subregional RTs among water parcels at different sewage outlets or among pollutants leaking at different locations in an irregularly shaped bay. In this study, following the concept of "partial age" proposed by Mouchet et al. (2016), we named the subregional RTs as the "partial residence times," which were used to partition the amount of time a water parcel spends in each subregion until the parcel leaves the control region. We extended the method developed by Delhez et al. (2004), using an adjoint approach to avoid the high computational cost in resolving the advection–diffusion problem, to calculate the continuous spatial distribution of "partial residence times."

This paper is organized as follows. The concept of partial residence times (PRTs) is introduced in Section 2. The diagnostic method for PRTs using the adjoint method is introduced Section 3. In Section 4, the PRT diagnostic method is validated using an analytical solution in an idealized 1D channel. In Section 5, a PRT application in a 3D tide-dominated bay (Jiaozhou Bay), which is divided into six functional subregions, is presented. Finally, a brief conclusion is provided in Section 6.

2 Concepts

2.1 Timescales for a single particle

As previously mentioned, the RT is defined as the amount of time a water parcel spends in a given control region before leaving (Bolin and Rodhe 1973; Takeoka 1984). To introduce the concepts of RT and PRTs, an idealized system is used, and it is schematized in Fig. 1. As the schematic diagram shows, a semi-enclosed bay ω consists of four nonoverlapping subregions ω_1–ω_4. Assuming that a particle is released at time t_0 within a bay, the particle moves through the control region (i.e., the bay) until arriving at the open boundary of the control region (the red dashed line in Fig. 1) at time t_5; then, the particle leaves the bay. Thus, according to the definition, the water particle RT is t_5–t_0. In fact, the particle has visited all four subregions (in the schematic diagram case) before moving out of the bay, and the particle has spent different amounts of time in different subregions. Here, we define the PRT_i as the amount of time the particle spends in the corresponding subregion ω_i from when the particle is released until it leaves the control region ω. According to the PRT definition, one can derive the following equations:

$$\begin{cases} \mathrm{PRT}_1 = t_1 - t_0 \\ \mathrm{PRT}_2 = (t_2 - t_1) + (t_5 - t_4) \\ \mathrm{PRT}_3 = t_3 - t_2 \\ \mathrm{PRT}_4 = t_4 - t_3 \end{cases} \tag{1}$$

The sum of the four PRTs is t_5–t_0, which equals the RT, i.e.,

$$\mathrm{RT} = \sum_{i=1}^{n} \mathrm{PRT}_i \tag{2}$$

where n is the number of subregions. Using the PRTs, we can effectively understand the RT composition in different subregions and obtain new insights into different particle influences in different subregions.

2.2 Mean residence time

Timescales related to a single particle undoubtedly have an explanatory value but are irrelevant for practical purposes (e.g., van Sebille et al. 2018). This is why averages over a

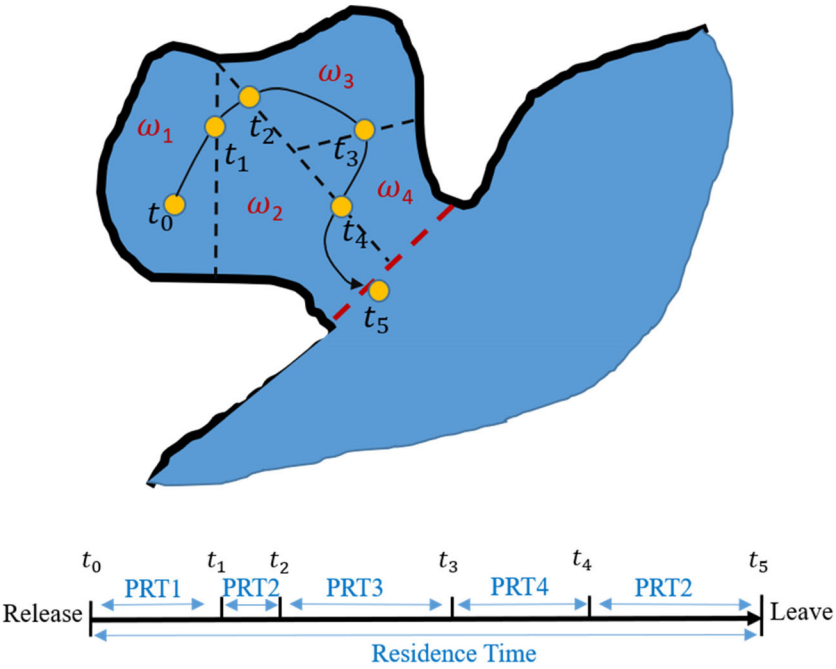

Fig. 1 Schematic diagram of the PRT concept. In the upper panel, the red dashed line denotes the open boundary of the control region ω. The control region ω is partitioned into four nonoverlapping subregions ω_1–ω_4 by the black dashed lines. A particle flows out of the control region along the trajectory denoted by the black solid line. The particle reaches the subregion boundaries at times t_1, t_2, t_3, and t_4 and, finally, reaches the control region boundary at time t_5. The lower panel denotes a coordinate with respect to the particle movement time. The partial residence times (PRT1–PRT4) in each subregion and RT are labeled in the time coordinate

sufficiently large number of particles must be evaluated (e.g., Takeoka 1984; Delhez et al. 2004). Following Takeoka (1984), the mean RT $\overline{\theta}(\mathbf{x}_0, t_0)$ at location $\mathbf{x}_0$ and release time t_0 can be expressed by integrating the tracer concentration in the control region in an Eulerian framework as follows:

$$\overline{\theta}(\mathbf{x}_0, t_0) = \int_{t_0}^{\infty} r(t)\mathrm{d}t \tag{3}$$

where $r(t) = \frac{m(t)}{m_0}$ is the remnant function, m_0 is the mass of the tracer initially released at location $\mathbf{x}_0$ and time t_0, and $m(t)$ is the tracer mass remaining in the control region (ω) at time t. The tracer mass in the control region can be calculated by simulating the transport of a conservative passive tracer, i.e.,

$$\begin{cases} \dfrac{\partial C}{\partial t} + \mathbf{v}\cdot\nabla C = \nabla\cdot[\mathbf{K}\cdot\nabla C] \\ C(\mathbf{x}_0, t_0) = m_0\delta(\mathbf{x}-\mathbf{x}_0) \end{cases} \tag{4}$$

where C is the tracer concentration, $\mathbf{v}$ is the velocity field, $\mathbf{K}$ is the diffusion tensor, and δ is the Dirac delta function. The value of m_0 does not affect the RT result and thus can be set to 1 (Delhez 2004). For the RT, re-entry is not considered; thus, the tracer concentration outside the control region is set to 0, i.e., $C(\mathbf{x} \notin \omega, t) = 0$ (Delhez and Deleersnijder 2006). If no boundary condition is prescribed at the open boundary of the control region, the result derived is actually the "exposure time," which includes re-entry; however, the boundary of the model domain should be set sufficiently far from the open boundary of the control region (Delhez 2013).

Finally, the mass of tracer m can be calculated by integrating C in the control region ω. Once concentration $C(\mathbf{x}, t)$ is obtained from the solution of partial differential problem (4), $\overline{\theta}(\mathbf{x}_0, t_0)$ can be derived from (3) as follows:

$$\overline{\theta}(\mathbf{x}_0, t_0) = \frac{\int_{t_0}^{\infty}\iiint_{\omega} C(\mathbf{x}, t)\,\mathrm{d}\mathbf{x}\mathrm{d}t}{\iiint_{\omega} C(\mathbf{x}, t_0)\,\mathrm{d}\mathbf{x}} = \int_{t_0}^{\infty}\iiint_{\omega} C(\mathbf{x}, t)\,\mathrm{d}\mathbf{x}\mathrm{d}t \tag{5}$$

2.3 Mean partial residence time

In reality, $\iiint_{\omega} C(\mathbf{x}, t)\,\mathrm{d}\mathbf{x}$ in Eq. (5) denotes the total tracer mass in the control region ω, which determines the RT in ω. The control region consists of nonoverlapping n subregions, i.e., $\omega = \bigcup_{i=1}^{n} \omega_i$ and $\omega_i \cap \omega_j = \varnothing\ (i \neq j)$. Therefore, we can separate $\iiint_{\omega} C(\mathbf{x}, t)\,\mathrm{d}\mathbf{x}$ into the components of different subregions as follows:

$$\iiint_{\omega} C(x, t)\,\mathrm{d}\mathbf{x} = \sum_{i=1}^{n}\iiint_{\omega_i} C(x, t)\,\mathrm{d}\mathbf{x} \tag{6}$$

According to the definition of the RT in Eq. (5), we can integrate the different components over time and derive the expressions for the RT components in different subregions, i.e., the PRT $\overline{\theta}_{\omega_i}$, yielding

$$\overline{\theta}_{\omega_i}(\mathbf{x}_0, t_0) = \int_{t_0}^{\infty}\iiint_{\omega_i} C(\mathbf{x}, t)\mathrm{d}\mathbf{x}\mathrm{d}t \tag{7}$$

Equation (7) is the forward solution of the PRT based on the remnant function method. In fact, PRTs can also be

interpreted as RT weights in each subregion. An expression similar to Eq. (7) was used by de Brauwere et al. (2011) in a study on the connectivity between different sections within an estuary, with the exception that de Brauwere et al. (2011) solved a 2D problem.

According to Eqs. (5–7), one can derive the RT by means of formula

$$\overline{\theta}(\mathbf{x}_0, t_0) = \sum_{i=1}^{n} \overline{\theta}_{\omega_i}(\mathbf{x}_0, t_0) \tag{8}$$

which means that the sum of the PRTs of all subregions equals the RT and is consistent with the PRT concept for the one-particle case.

In the calculation of the PRT, the concentration equation is relation (4), which is exactly the same as that used to calculate the RT. The boundary conditions for the PRT should also remain exactly the same as those for the RT, i.e., there is only one open boundary condition with $C = 0$ for the control region ω, and there is no boundary condition for the boundaries between adjacent subregions (i.e., the black dashed lines in Fig. 1). The boundary conditions are consistent with the physical meaning of the PRT, i.e., that the water parcel can re-enter the subregions within the control region (e.g., PRT2 in Fig. 1) and cannot re-enter the control region when it leaves the open boundary of the control region.

3 Determination of PRTs using the adjoint method

3.1 Equation for the residence time

Based on the concept introduced in this study, PRTs can be determined using the particle-tracking method by recording the amounts of time particles spent in different subregions or the remnant function method, as shown in Eqs. (4) and (7). However, the number of particles must be sufficiently large so that the Lagrangian solution is close to that of the Eulerian problem (e.g., Silverman 1986; Spivakovskaya et al. 2007), which is not always the case. This is partly because there is no truly reliable criterion for estimating a priori the number of particles to be seeded. Additionally, both the particle-tracking and the remnant function methods cannot easily characterize the continuous spatiotemporal variations in the RT and PRTs because a large computational cost is required to run the model (e.g., Delhez et al. 2004; Du and Shen 2016). When using the two approaches, the number of model runs needed is equal to the number of points where and times when the RT and PRTs are to be evaluated, implying that the CPU time can be prohibitive. To address this issue, Delhez et al. (2004) proposed the adjoint method for the RT to derive the continuous spatiotemporal variations in the RT with only one computation. Therefore, in this section, we introduce the RT adjoint method proposed by Delhez et al. (2004), and then, we extend the adjoint method to determine PRTs.

Delhez et al. (2004) derived the adjoint form of the forward problem, i.e., Eqs. (4–5), leading to the equation obeyed at any time and position by the residence time:

$$\frac{\partial \overline{\theta}}{\partial t} + \delta_\omega(\mathbf{x}) + \mathbf{v}\cdot\nabla\overline{\theta} + \nabla\cdot\left[\mathbf{K}\cdot\nabla\overline{\theta}\right] = 0 \tag{9}$$

where $\delta_\omega(\mathbf{x})$ is the characteristic function of the control region ω and $\delta_\omega(\mathbf{x}) = \begin{cases} 1 & \forall \mathbf{x}\in\omega \\ 0 & \forall \mathbf{x}\notin\omega \end{cases}$. The detailed derivation was introduced by Delhez et al. (2004). Notably, Eq. (9) must be integrated backward in time to solve for $\overline{\theta}$ (Delhez et al. 2004). The RT values are set to 0 under the initial conditions (Delhez 2006).

The boundary conditions for Eq. (9) are presented in Table 1. For the RT, $\overline{\theta}$ must vanish at the boundary of the control region (red dashed line in Fig. 1). Therefore, the open boundary is assigned a homogeneous Dirichlet boundary condition, i.e., $\overline{\theta} = 0$, which reflects the time required to exit the control region for the first time (Delhez et al. 2004; Delhez 2006; Delhez and Deleersnijder 2006). Although this condition could induce the development of boundary layers (at the inflow boundaries of $\overline{\theta}$) and generate spurious oscillations near this (Delhez and Deleersnijder 2006; Blaise et al. 2010), the boundary condition of $\overline{\theta} = 0$ is practical because the value of the RT near the boundaries is usually relatively small and the influence of the oscillation on the RT results is insignificant in many cases (e.g., Du and Shen 2016). In addition, if the re-entry process is considered in the time a water parcel spends in the control region, i.e., the exposure time (ET), no boundary conditions need to be prescribed on the open boundaries of control region ω. However, the boundary condition of $\overline{\theta} = 0$ needs be prescribed on the boundary of the computational domain (Delhez 2006).

Table 1 Boundary conditions for the RT and PRT equations from the adjoint method

For	Boundary conditions	Expressions
RT and PRT	Open boundary of ω	$\overline{\theta} = 0$ (B1)
RT and PRT	Closed boundary of ω	$\vec{\mathbf{n}}\cdot(\nabla\overline{\theta}) = 0$ (B2)
RT, ET, and PRT	Boundaries of the computational domain	$\overline{\theta} = 0$ (B3)
PRT	Boundaries between subregions within ω	/

$\vec{\mathbf{n}}$ is the outgoing unit vector normal to the boundary

3.2 Equations for the partial residence times

In Eq. (9), the characteristic function $\delta_\omega(\mathbf{x})$ delineates the control region ω, i.e., the region in which the time spent is to be evaluated (Delhez et al. 2004). Therefore, to record the time spent in only one subregion ω_i, we must change the characteristic function $\delta_\omega(\mathbf{x})$ into the characteristic function for the subregion $\delta_{\omega_i}(\mathbf{x})$. The PRT for subregion ω_i can be determined as follows:

$$\frac{\partial \overline{\theta}_{\omega_i}}{\partial t} + \delta_{\omega_i}(\mathbf{x}) + \mathbf{v}\cdot\nabla\overline{\theta}_{\omega_i} + \nabla\cdot\left[\mathbf{K}\cdot\nabla\overline{\theta}_{\omega_i}\right] = 0 \tag{10}$$

where $\delta_{\omega_i}(\mathbf{x})$ is the characteristic function for subregion ω_i and $\delta_{\omega_i}(\mathbf{x}) = \begin{cases} 1 & \forall \mathbf{x}\in\omega_i \\ 0 & \forall \mathbf{x}\notin\omega_i \end{cases}$. Equation (10) is derived from an adjoint method similar to that of Delhez et al. (2004). The detailed derivation of Eq. (10) is given in the Appendix.

The initial PRT values are set to 0. The boundary conditions for Eq. (10) are listed in Table 1. For the PRTs, no boundary conditions need to be prescribed on the boundaries separating the subregions because a water parcel might reenter one subregion before leaving the control region (e.g., Fig. 1). At the boundary of the control region, the boundary conditions for the PRTs and the RT are similar.

By summing Eq. (10) for the n subregions, one obtains

$$\frac{\partial \sum_{i=1}^{n} \overline{\theta}_{\omega_i}}{\partial t} + \sum_{i=1}^{n} \delta_{\omega_i}(\mathbf{x}) + \mathbf{v}\cdot\nabla\left[\sum_{i=1}^{n} \overline{\theta}_{\omega_i}\right] + \nabla\cdot\left\{\mathbf{K}\cdot\nabla\left[\sum_{i=1}^{n} \overline{\theta}_{\omega_i}\right]\right\} = 0 \tag{11}$$

Since $\omega = \bigcup_{i=1}^{n} \omega_i$ and $\omega_i \cap \omega_j = \varnothing\ (i \neq j)$, the sum of the characteristic functions for the subregions equals the characteristic function for the control region, i.e.,

$$\sum_{i=1}^{n} \delta_{\omega_i}(\mathbf{x}) = \delta_\omega(\mathbf{x}) \tag{12}$$

Taking the sum of Eq. (11) on all the subdomains, using relation (12) and keeping in mind that the boundary conditions for the RT and the PRTs are similar, it follows that the RT is, as expected, equal to the sum of the PRTs, i.e., $\overline{\theta}(x_0, t_0) = \sum_{i=1}^{n} \overline{\theta}_{\omega_i}(x_0, t_0)$.

3.3 Implementation in the numerical model

Equations (9) and (10) have forms similar to the tracer transport equation, except that the diffusion term has the opposite sign and the term $\delta_\omega(\mathbf{x})$ is added. Therefore, in this study, RT and PRT diagnostic models are established based on the module for calculating the tracer transport in the Marine Environment Research and Forecasting (MERF) ocean model (Liu et al. 2016). Characteristic functions $\delta_\omega(\mathbf{x})$ and $\delta_{\omega_i}(\mathbf{x})$ are added to the modules for the RT and PRTs models. In the models, Eqs. (9) and (10) are solved using the finite difference method. The second-order centered difference is used in diffusion term discretization. For stability, the implicit central difference method is used to solve the vertical diffusion term. A total variation diminishing scheme with a Superbee and HSIMT alternating flux limiter (TVDal) developed by Lin and Liu (2019) is used in advection term discretization. The TVDal scheme has a numerical error that is smaller than that of conventional TVD schemes, especially for long-term integrations (Lin and Liu 2019).

The RT or PRT fields at the instant the backward time integration begins are unknown. This is why a spin-up period is necessary, which, according to Delhez (2006), must be at least twice as long as the maximum value of the RT in the domain of interest. In the experiments in this study, the flow fields are tidal periodic; thus, the RT and PRT values should also be periodic. We integrated the RT and PRT models until stable variations in the RT and PRTs at the tidal frequency were observed, and all the integration times were much longer than twice the longest RT in the control region in the corresponding experiments.

4 Validation for an idealized 1D channel

In Section 3, we derived the diagnostic equation for PRTs using the adjoint method, and the model for PRTs was established based on this equation. To validate the equation and the model for PRTs, a test is conducted in an idealized 1D channel with idealized tidal currents. First, the experimental setting and the analytical solution for the PRTs are introduced. The analytical solution is directly derived from the forward process of the movement of particles. Then, the modeled PRTs are compared to the analytical solution to verify the reliability of the diagnostic equation and model of PRTs.

4.1 RT and PRTs for an idealized 1D channel

As shown in Fig. 2, the experiment involves an idealized channel with a constant depth and width. In the channel, there is a uniform tidal current $u(t) = U\sin(2\pi t/T)$ with amplitude U and period T. Generally, the residual current determines the subtidal transport in a tidal-dominated marine system (Feng et al. 1986). Therefore, a constant residual current Rc is superposed on the tidal current. For simplicity, diffusion is assumed to be negligible.

One can track a water particle located at $x(t_0)$ from instant t_0 onwards. Subsequently, the particle moves with the flow.

Therefore, we can derive the particle location in the channel at time t as follows:

$$\begin{aligned} x(t) &= x(t_0) + \int_{t_0}^{t} U\sin(2\pi t/T)\,\mathrm{d}t + Rc\cdot(t-t_0) \\ &= x(t_0) + (UT/2\pi)[\cos(2\pi t_0/T) - \cos(2\pi t/T)] + Rc\cdot(t-t_0) \end{aligned} \quad , t_0 \le t \le +\infty \tag{13}$$

Under the homogeneous Dirichlet boundary condition, the particle RT is the amount of time the particle spends in the control region before leaving. In the idealized test, the interval ($(L_1 \le x \le L_2)$) is set as the control region within the channel. Based on the formula for $x(t)$, we can derive the RT as that when $x(\mathrm{RT} + t_0) = L_1$ or L_2 for the first time.

One can track the water particle at different locations in the domain interval from different instances onwards. Then, to find the time when the particles exit the control region according to Eq. (13), we can obtain the RT analytical solution. Assuming that the channel consists of two subregions, i.e., subregion 1, $L_1 \le x \le L_M$, and subregion 2, $L_M \le x \le L_2$, the PRTs in each subregion are derived by separating the time spent in the two subregions using the same method as that for the RT.

4.2 Comparison between the modeled RT and PRTs and analytical solutions

In the idealized test, the channel length is set to 80 km. The detailed configuration of the channel experiment is summarized in Table 2. The RT and PRT diagnostic models are used to calculate the RT and PRTs in the two subregions. The channel is discretized in the models with a 100-m uniform grid spacing. The time step is set to 10 s. The RT and PRT analytical solutions at the centers of each grid are used for comparison with the RT and PRT modeled grid results.

The RT results at time = 0 show that the RT decreases from left to right due to a rightward-moving residual current (Fig. 3a, b). A very low RT occurred near 60 km because the water can exit the control region during the first tidal cycle. PRT1 is 0 in subregion 2, i.e., the 30 km $\le x \le$ 60 km interval, which indicates that the water in subregion 2 could not move into subregion 1 due to the rightward-moving residual current. Therefore, the subregion 2 RT is contributed by PRT2. However, subregion 1 water must move through subregion 2 to exit the control region. Therefore, the subregion 1 RT consists of PRT1 and PRT2. The RT and PRT results also display tidal variations (Fig. 3c–f). For the water parcel at $x = 20$ km, the RT and PRT1 are time varying, and PRT2 is constant, which indicates that the RT temporal variation is induced by the variation in PRT1 (Fig. 3c, d). However, for the water parcel at $x = 30$ km, both PRT1 and PRT2 contribute to the temporal variation in RT (Fig. 3e, f). In summary, the RT and PRT diagnostic models obtain results that are consistent with the analytical solution (Fig. 3). The relative biases of both the RT and PRT between the modeled results and analytical solution are less than 1%. Therefore, the RT and PRT diagnostic equation and model introduced in Section 3 is reliable for practical cases.

Table 2 Configuration of the experiment for the 1D idealized channel

Parameter	T (h)	U (m/s)	Rc (m/s)	L_1 (km)	L_2 (km)	L_M (km)
Value	12	0.5	0.01	10	60	30

5 Application to a realistic case—Jiaozhou Bay

In this section, the PRT diagnostic method is applied to tide-dominated Jiaozhou Bay (JZB), which is divided into six functional subregions. The PRTs in the six subregions are computed, showing that more detailed information and new insights into the water exchange can be obtained using the PRT concept.

5.1 Study area and model description

5.1.1 Study area

JZB is a typical semi-enclosed bay located on the west coast of the Yellow Sea (Fig. 4). The average water depth of JZB is approximately 7.5 m. The maximum water depth is ~60 m near the bay mouth. There is a large area of tidal flats (~1/4 of the total area) in JZB. The water motion in JZB is dominated by tides (e.g., Lv et al. 2010; Shi et al. 2011; Liu et al. 2012a): the semidiurnal M_2 tide provides over 80% of the total energy of the seawater (Ding 1992). The wind over JZB is relatively weak, with an annual average wind speed of 5.4 m/s (Editorial Board of Annals in China 1993). Several small rivers discharge along the JZB coast, which is the major way for urban

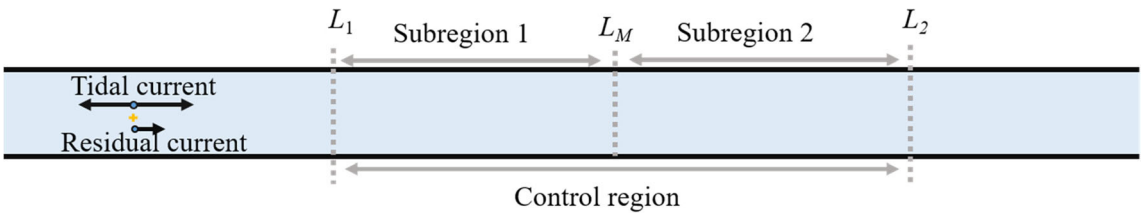

Fig. 2 Schematic diagram of the idealized 1D channel with tidal currents and a residual current

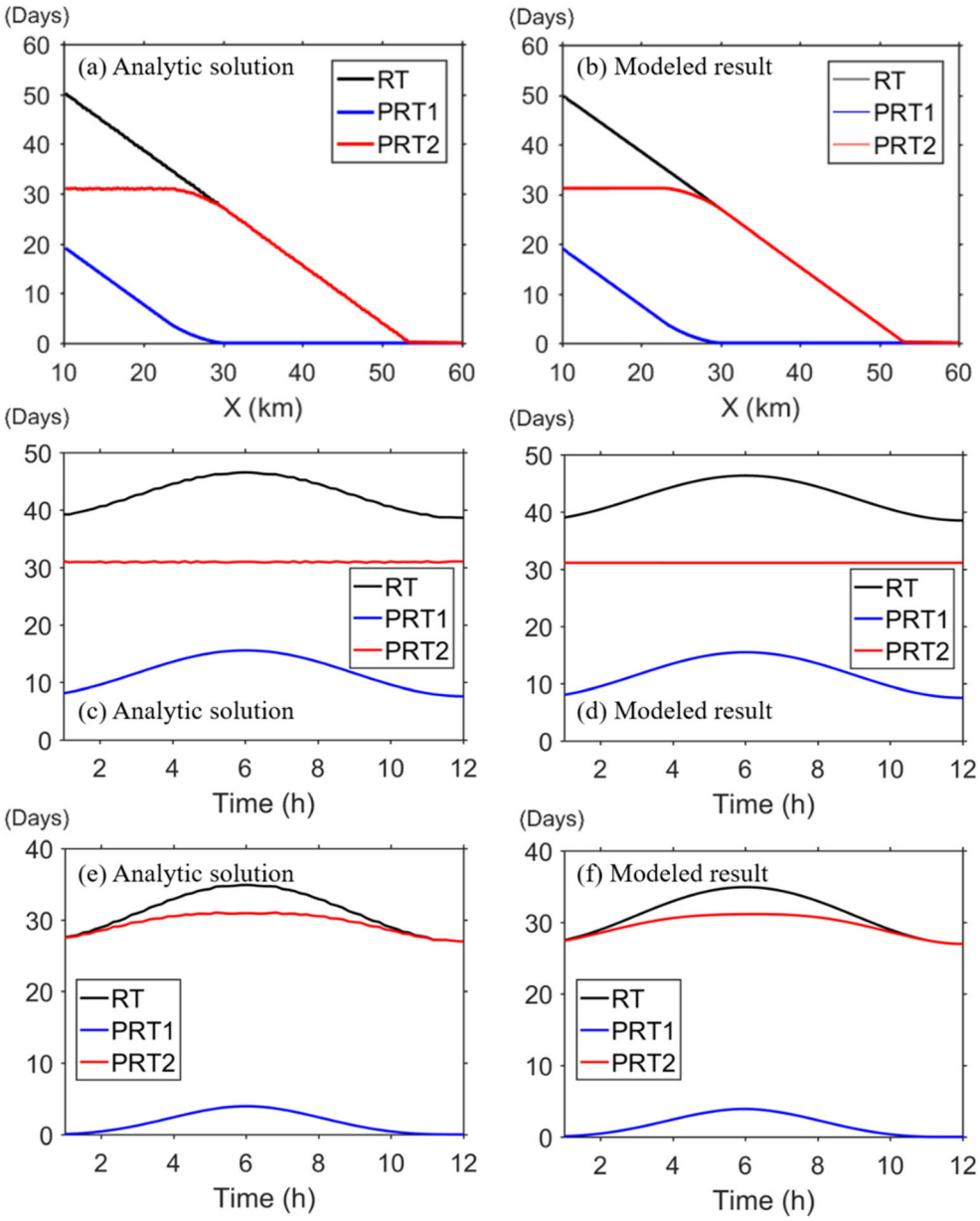

Fig. 3 RT and PRT results for the idealized 1D channel. PRT1 and PRT2 denote the PRTs in subregions 1 and 2, respectively. The left figures are the analytic solutions, and the right figures are the model results. **a**, **b** The results along the channel at time = 0. **c**, **d** The results for $X = 20$ km in one tidal cycle. **e**, **f** The results for $X = 30$ km in one tidal cycle

sewage discharge. The seven major rivers are the Xinan River, Yang River, Dagu River, Moshui-Baisha River, Loushan River, Licun River, and Haibo River, which are denoted by black stars with nos. 1 to 7 in Fig. 4. However, the river discharge is very limited ($< 2 \times 10^6$ m^3 day^{-1}) and much less than the tidal prism ($\sim 0.9 \times 10^9$ m^3) (Lin et al. 2016); thus, the influence of river discharge on the hydrodynamics of JZB is negligible (e.g., Liu et al. 2012a).

JZB is surrounded by the city of Qingdao, which has a population of several million people. JZB has one large harbor (Qingdao Harbor) within the bay and a large area of aquacultural farms. In terms of multifunctional uses, JZB is divided into different functional zones (e.g., Zheng 1994). According to the marine functional zoning and environmental characteristics of JZB (Zheng 1994; Qingdao Marine Environment Bulletin 2017), the JZB domain is roughly partitioned into six subregions, which are shown in Fig. 4. The mean area, mean volume, and functions of the six subregions are provided in Table 3. The largest tidal current in JZB exists in the mouth of the bay and is induced by the narrowness of the channel and the presence of a sharp headland (Lin et al. 2015). The anchorage zone has the maximum volume of the six subregions due to the deep water depth there. The estuarine zone is outside the Dagu River, which has the largest runoff into JZB and can transport rich nutrients to JZB, especially during summer. Subregion ω_6, located in the northeastern JZB area, is eutrophic and polluted with heavy metals (Qingdao Marine Environment Bulletin 2017).

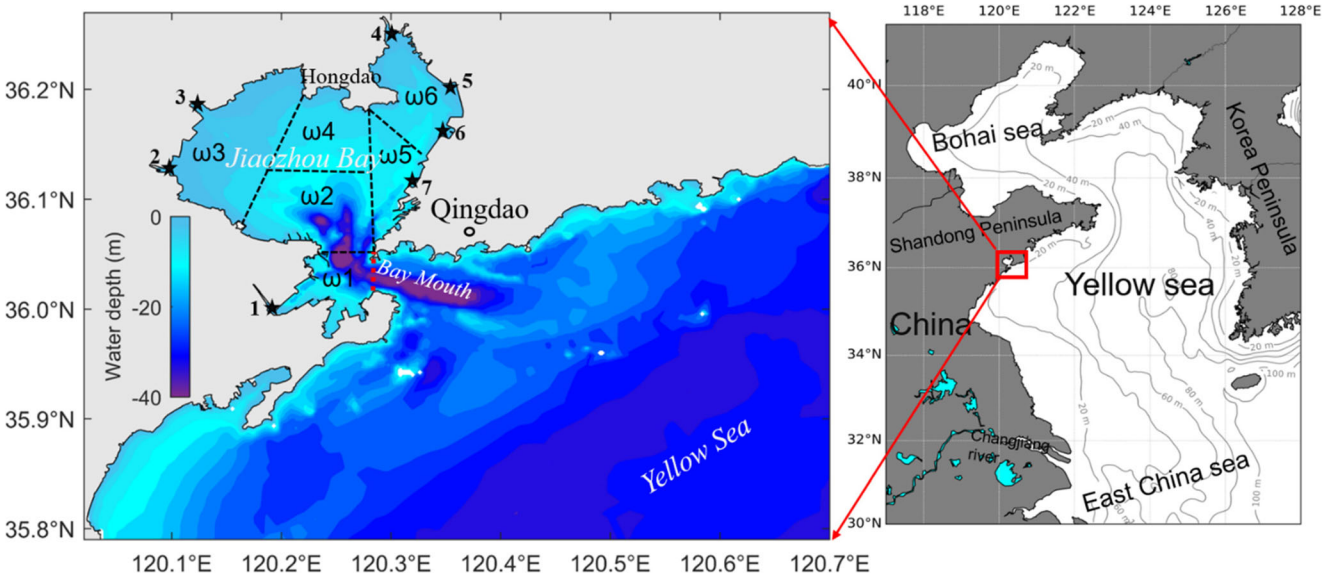

Fig. 4 Jiaozhou Bay topography, domain for the hydrodynamic model, and RT and PRT diagnostic models. The red dashed line at the bay mouth denotes the open boundary of the control region. The black dashed lines denote the boundaries of six subregions (i.e., ω_1–ω_6). The black stars labeled nos. 1–7 denote the estuaries of the seven major rivers, i.e., the Xinan River, Yang River, Dagu River, Moshui-Baisha River, Loushan River, Licun River, and Haibo River

5.1.2 Hydrodynamics model

To focus on the tidal effect on the timescales of water transport, only the tide (the M_2 constituent) was considered in the hydrodynamic model of JZB, and a JZB barotropic tidal hydrodynamics model was used to simulate the tide, as in previous studies of JZB (e.g., Liu et al. 2004; Lv et al. 2010; Shi et al. 2011; Lin et al. 2015). The JZB tidal model developed by Liu et al. (2012a) was used to provide the flow field for the RT and PRT models. The model was set up based on the Princeton Ocean Model (POM) with wetting and drying capabilities (Oey 2005; Oey 2006; Blumberg and Mellor 1987). The modeling zone was discretized into 312 × 213 grids with an approximately 200 × 250 m horizontal resolution and 17 uniform layers in the vertical direction. On the open boundary, the M_2 surface elevation was prescribed, with the amplitude and phase obtained from the marine atlas of Chen (1992). A homogeneous and constant salinity and temperature were used in the model. The simulated tidal current and elevation were validated by Liu et al. (2012a) and Lin et al. (2015). Additional model and tidal flow details can be found in the studies of Liu et al. (2012a) and Lin et al. (2015).

5.1.3 Set up of the RT and PRT simulations

Based on Eqs. (3) and (4), RT and PRT diagnostic models for JZB were established. The models used the same grids and layers as the JZB hydrodynamics model. In the RT and PRT models, the JZB mouth is set as an open boundary of the control region (red dashed line in Fig. 4). Because of the existence of tidal flats, the control region varies with flooding and ebbing. In the RT and PRT models, the control region includes only the wet grids in JZB. The advection–diffusion component of the RT and PRT models used a wetting–drying method similar to that in the hydrodynamics model, i.e., POM (Oey 2005). During the computation, the characteristic functions $\delta_\omega(\mathbf{x})$ are equal to 1 in the wet grids within the control region and 0 in the dry grids. To calculate the RT and PRTs in

Table 3 Information of the six subregions in JZB

Subregions	Marine functions and characteristics	Area (km^2)	Volume (km^3)	Area/total (%)	Volume/total (%)
ω_1	Bay mouth zone	39.58	0.63	12.3	25.1
ω_2	Anchorage zone	75.88	1.04	23.7	41.5
ω_3	Estuarine zone	78.14	0.16	24.4	6.2
ω_4	Aquiculture zone	48.81	0.26	15.2	10.5
ω_5	Port and industrial zone	34.06	0.25	10.6	10.0
ω_6	Eutrophic and heavy polluted zone	44.31	0.15	13.8	6.1

JZB, we first ran the hydrodynamic model for 30 days until we obtained stable variations in the tidal currents at the tidal frequency. The velocity and turbulence diffusion coefficient fields were outputted and saved every 6 min for only the last tidal cycle due to tidal flow recycling. Then, we ran the diagnostic models by backward recycling the saved velocity and turbulent diffusion coefficient fields as inputs. Stable variations in RTs and PRTs were observed after ~300 days of modeling. Finally, to further eliminate the effect of the initial conditions, the RT and PRT results on the 600th day were outputted and analyzed.

5.2 RT in JZB

The modeled RT and PRT results in JZB are shown in Figs. 5 and 6. Due to the tidal recycling of RT and PRTs, we show only the mean results for the RT and PRTs in one tidal cycle on the 600th day. Generally, the RT increases from the JZB mouth to the top of the estuary (Fig. 5a). Two regions of high RT (> 110 days) occurred along both the east and west sides of Hongdao. The average RT is ~39 days and is mostly consistent with the values from previous studies that used the particle-tracking method or the remnant function method. For instance, using the particle-tracking method, Wang et al. (2009) found that the RT is of the order of 36 days in JZB. Liu et al. (2004) and Shi et al. (2011) computed the RT in JZB using the remnant function method and obtained values of ~52 and ~41 days, respectively. The results of this study are very close to the results of Wang et al. (2009) and Shi et al. (2011), and the RT from Liu et al. (2004) is ~10 days longer, which may be caused by the fact that wetting–drying of tidal flats was not taken into account in Liu et al. (2004). The similar RT results verify the reliability of the RT model in this study. The maximum RT in JZB from all studies is longer than 100 days at the top of JZB, indicating weak exchange in the inner JZB, which is related to the weak tidal–residual current (Liu et al. 2012a).

5.3 PRTs in JZB

The PRTs in the six subregions show significant spatial inhomogeneities, especially in subregions ω_3, ω_4, and ω_6, which are located at the top of JZB (Fig. 6). High values of PRT3, PRT4, and PRT6 occur in the corresponding subregions, i.e., ω_3, ω_4, and ω_6, respectively. The PRT maximum in these three subregions can reach more than 60 days, indicating a long residence of water within the subregions. However, PRT1, PRT2, and PRT5 are relatively short, which suggests that the water in JZB can quickly move through subregions ω_1, ω_2, and ω_5. This result is understandable because strong exchange occurs at the JZB mouth and in the adjacent waters due to the strong tidal current.

In addition, the sum of the PRTs basically equals the RT, with a small mean bias of ~2% (Fig. 5a, b). The small bias is likely related to the numerical error from using multiple tracers and the nonlinear advection discretization scheme for PRTs. The model results are consistent with the PRT concept that the sum of the PRTs in all subregions should equal the RT, which indirectly demonstrates the reliability of the PRT method when complex flows and diffusion are to be taken into account.

Based on the PRT results, we can decompose the JZB RT into different components in each subregion, which can provide some new insights into the RT and water exchange process. We take the RTs at some specific locations as examples (Fig. 7). The residence of river water in a bay may be of great concern to ecological researchers and environmental managers, as rivers usually bring nutrients and pollutants into bays. As shown in Fig. 7a, the seven estuaries display different RTs in JZB, ranging from ~70 to ~150 days. In addition, the estuaries have very different PRTs. For example, the RT of the no. 1 estuary is mainly PRT1 (> 75%), and the RTs of other estuaries have very low PRT1 values (< 5 days). This finding suggests that estuarine water can move very quickly through subregion 1, except for the no. 1 estuary. For the no. 2 and 3 estuaries, the RT consists of PRT2 and PRT3, which suggests that the river water could have relatively long RTs in

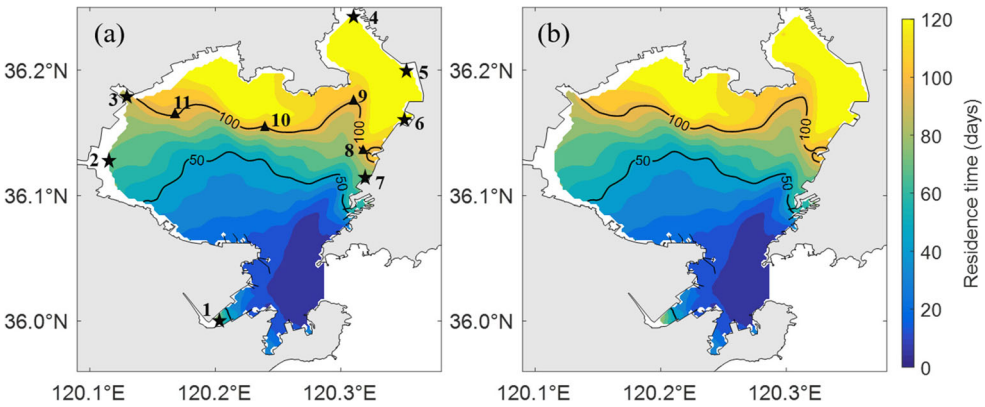

Fig. 5 RT tidal mean (**a**) and sum of six PRTs (**b**). The stars (nos. 1–7) in **a** show the estuary locations of the seven major rivers along the JZB coast. The triangles (nos. 8–11) show the locations of four different water parcels with the same RT (100 days)

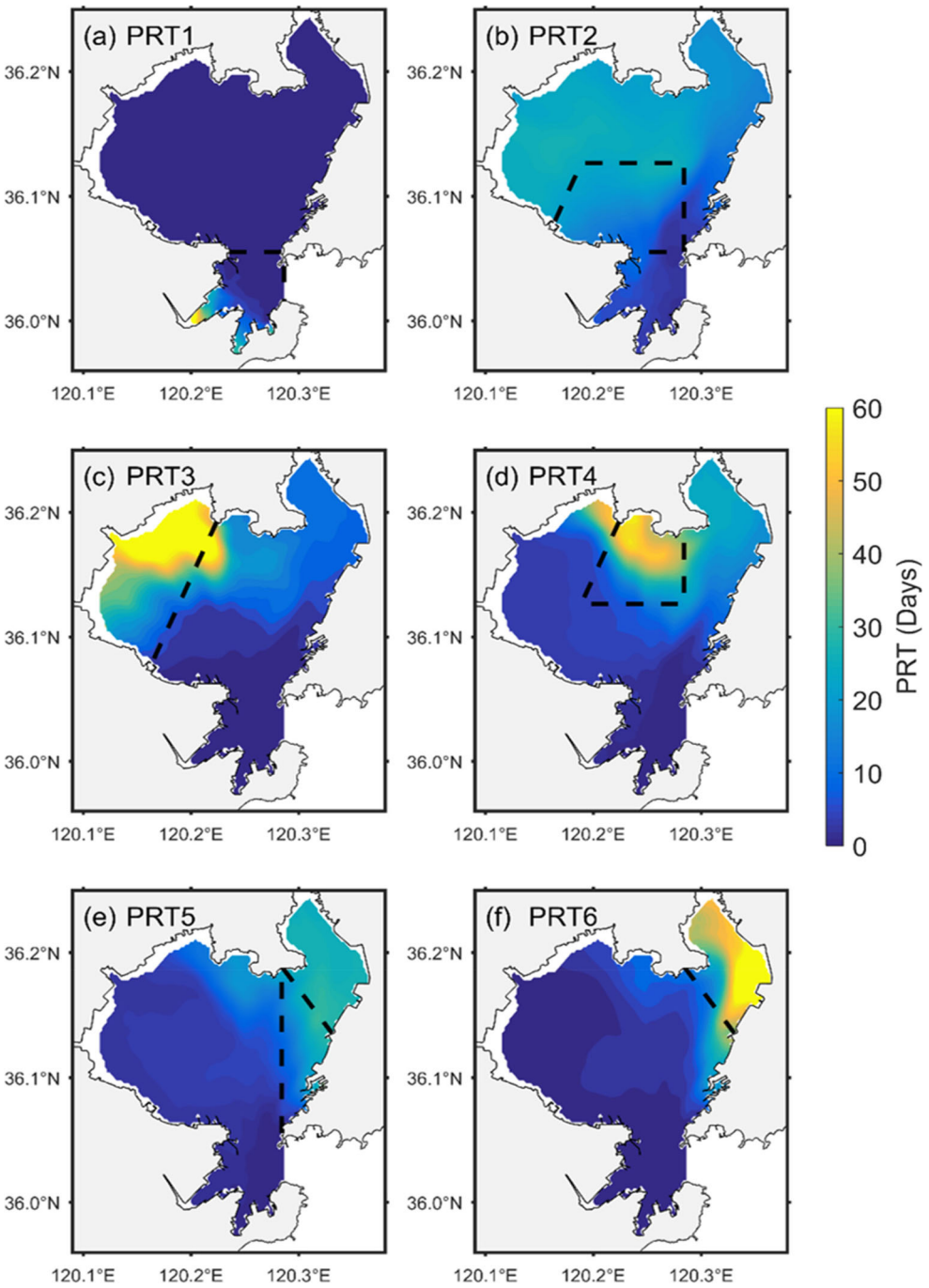

Fig. 6 **a**–**f** PRTs for the six subregions in JZB, i.e., ω_1–ω_6. PRT1–6 denote the times spent by the water parcel in subregions 1–6. The black dashed lines denote the boundaries of each subregion

subregions ω_2 and ω_3 and a very limited RT in the other subregions. For the no. 4–7 estuaries, PRT5 and PRT6 are the two main components of the RT in JZB, which indicates that the river water could influence subregions ω_5 and ω_6 for a relatively long period of time.

In addition, the PRTs for the four water parcels at different locations but with the same RT (100 days) are compared (Fig. 5a). The PRT results show that water parcels with the same RT have completely different PRT compositions (Fig. 7b), which indicates that the pathways out of the JZB are completely different, even though the particles spend the same amount of time moving through the bay. For example, no. 8 spends more than 60% of its time in subregions ω_5 and ω_6, and no. 11 only spends ~ 5% of its time in subregions ω_5 and ω_6, but no. 11 has a long travel time (90 days) through subregions ω_2 and ω_3.

5.4 Discussion

Based on the proposed PRT concept and method, the components of the RT in the different prescribed subregions of JZB

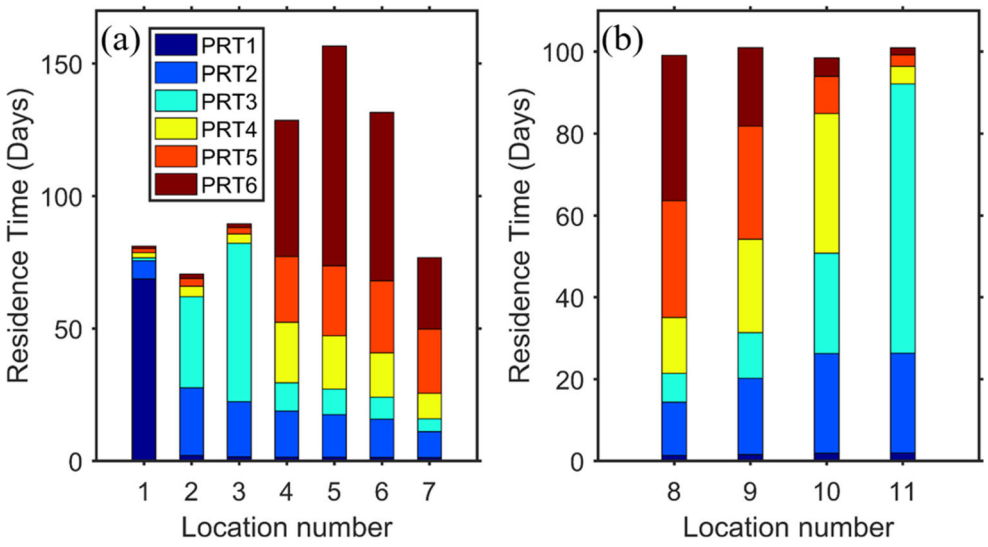

Fig. 7 RT compositions in each subregion for water in different locations (nos. 1–11 in Fig. 5a). Numbers 1–7 in **a** denote the estuaries of the seven major rivers along the JZB coast. Numbers 8–11 in **b** denote four different water parcels with the same RTs (~ 100 days)

were derived, which provided detailed information on the corresponding water transport processes. Due to the relatively weak wind and small freshwater discharge, the impact of the wind stress and dilution of freshwater on water exchange were neglected, and only tides were considered in the hydrodynamic model of JZB, as in previous studies of JZB (e.g., Liu et al. 2004; Lv et al. 2010; Shi et al. 2011; Lin et al. 2015). Therefore, the tide is the only forcing related to the RT and PRTs simulated in this study. However, the seasonal shifts in winds or some short-time extreme events (e.g., a typhoon or storm) could have some influence on the variations in the RT and PRT results and will be studied in a follow-up work.

The magnitude of the PRTs is related not only to the local hydrodynamics but also to the size of the subregions. Assuming that the capacity of water exchange is uniform in the control region, the PRT should be proportional to the volume of the corresponding subregion, and the PRTs divided by the volume of the corresponding subregions should be equal. Thus, to compare the water transport rate in different subregions and quantify the water exchange capacity of subregions, normalizing the PRTs by the volume of the corresponding subregion (NPRT) could be most appropriate. The NPRT is defined as the ratio of the PRT to the volume of the corresponding subregion, thereby representing the time spent by a water parcel in a unit volume of the subregion. Based on the results of the PRT and the volumes of subregions (Table 3), the NPRTs for the water parcels at location nos. 1–11 are derived as shown in Fig. 8. Notably, for nos. 1–11, NPRT3–6 have relatively higher values, and NPRT1–2 are much lower than the others. This finding indicates a fast transport rate in ω_1 and ω_2 and a relatively poor water exchange capacity in ω_{3-6}, especially in ω_3 and ω_6. In addition, the different NPRTs for nos. 1–11 in the same subregions reflect the different transport rates of subregions for different water parcels, which reflects the inhomogeneity of the flow field.

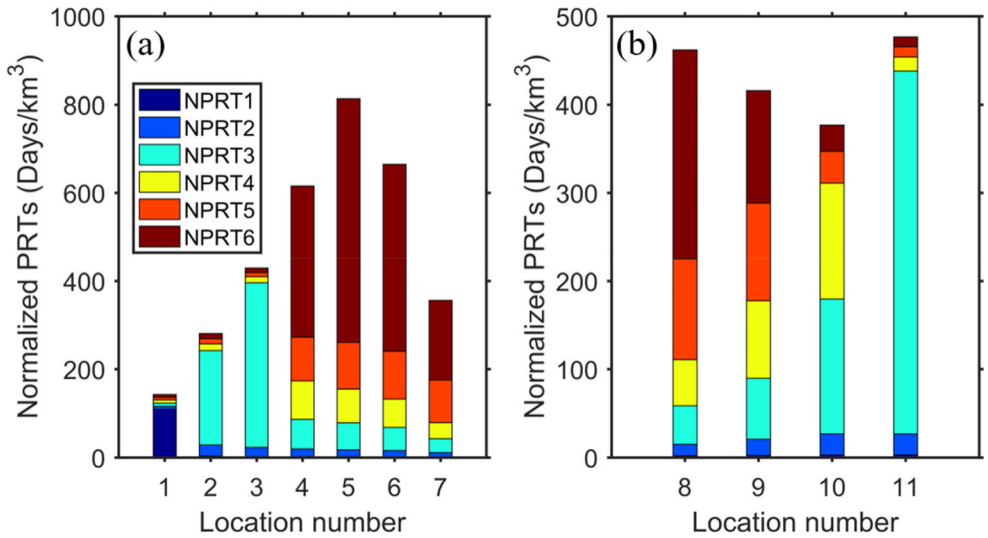

Fig. 8 As in Fig. 7, except the PRTs are normalized by the volume of the corresponding subregion (NPRT)

According to the Qingdao Marine Environment Bulletin (2017), subregions ω_3, ω_4, and ω_6 in JZB have severely polluted sea areas in summer when the river runoff is relatively large. Based on the PRT results in Fig. 7a, rivers 2 and 3 have a long PRT3 but very short PRT in other subregions, and river nos. 4, 5, and 6 have relatively large values of PRT4 and PRT6. The results suggest that the river water has a relatively long-term influence on the local region. Therefore, the environmental issues in ω_3 and ω_6 could be associated with the local sources of river nos. 2–3 and 4–6, respectively. For the middle subregion ω_4 with no river at the coast, the environmental problem is likely related to rivers (nos. 4–6) on the east coast, and the effect of rivers on the west coast on ω_4 is limited due to the much longer PRT4 for river nos. 4–6. In addition, the NPRT results show that ω_3, ω_4, and ω_6 have relatively poor water exchange capacities. Therefore, the PRT results indicate that the poor local exchange capacities and long-term residence of eutrophic river water could be the two leading causes of environmental issues in these subregions.

The application involving JZB shows that the PRT is helpful for understanding the water transport processes in different subregions within the control region and the water exchange capacity in subregions. Seas are commonly divided into many subregions; for instance, the Bohai Sea is partitioned into several sub-bays (e.g., Laizhou Bay, Bohai Bay, and Liaodong Bay) (Liu et al. 2012b), and the Chesapeake Bay consists of one main estuary and more than ten subestuaries (Gong et al. 2009). The PRT concept and method have the potential for application in these sea areas to better understand and evaluate the effects of multiple point pollution sources (e.g., sewage and oil spills) on different subregions, the water exchange capacity of subregions, and the connectivity among subregions (e.g. de Brauwere et al. 2011).

6 Conclusions

In this study, the concept of PRTs is proposed to determine the RT compositions in different subregions. PRTs are defined as the time spent by a water parcel in different subregions until leaving the control region. The adjoint method is used to compute the PRTs. A test is conducted in an idealized 1D channel to validate the PRT diagnostic method. In the test, the modeled PRTs are highly consistent with the analytical solution, which verifies the reliability and applicability of the PRT model. Finally, the PRTs in JZB, which consists of six subregions, are derived using the PRT model. PRTs in the estuaries of the seven major rivers clearly show different RT compositions in different subregions, and the results potentially quantify the influences of different rivers in different subregions.

The PRT concept and modeling results can provide detailed information and new insights into the water exchange process. The PRT concept and diagnostic method can also be used in studies of water exchange in estuaries, lakes, and reservoirs.

Acknowledgments The authors thank Profs. Lian Xie and Huiwang Gao of the Ocean University of China and Dr. John Keesing of CSIRO Oceans and Atmosphere Research, Australia, for their valuable suggestions. The authors also thank Editor Eric Deleersnijder and two anonymous reviewers for their very constructive comments that help us improved the manuscript. The authors declare that the research was conducted in the absence of any commercial or financial relationships that could be construed as potential conflicts of interest.

MERF has been upgraded from MERF-NH 2.0 (MERF Non-hydrostatic Version 2.0) to MERF-NH 2.1, primarily because of the adoption of the water age and residence time modules. For access to MERF-NH 2.1 and the associated data, please contact zliu@ouc.edu.cn.

Funding information This work was supported by the Special Fund for Public Welfare Industry (Oceanography) (grants 200805011 and 201205018).

Abbreviations *RT,* Residence time; *PRT,* Partial residence time; *PRTs,* Partial residence times; *ET,* Exposure time; *CART,* constituted-oriented age and residence time theory (https://www.climate.de/cart); *MERF,* Marine Environment Research and Forecasting ocean model; *TVDal,* Total variation diminishing scheme with an alternating flux limiter; *JZB,* Jiaozhou Bay; *POM,* Princeton Ocean Model

Derivation of the equation for PRT

Equation (10) is the backwards equation for the PRT, which can be derived by an adjoint method very similar to that Delhez et al. (2004) developed for obtaining the RT. Taking PRT_i in one of subregions ω_i as an example, the expression $\iiint_{\omega_i} C(x,t)\,\mathrm{d}x$ in the definition of the PRT [i.e., Eq. (7)], which can be solved efficiently using the adjoint form of Eq. (4). We can define the adjoint variable C_T^* satisfying the differential equation (additional details on the derivation of the adjoint problem are provided in Appendix A of Delhez et al. (2004)):

$$\begin{cases} \dfrac{\partial C_T^*}{\partial t} + \mathbf{v}\cdot\nabla C_T^* + \nabla\cdot\left[\mathbf{K}\cdot\nabla C_T^*\right] = 0 \\ C_T^*(x,T) = \delta_{\omega_i}(x) \end{cases} \tag{14}$$

where $\delta_{\omega_i}(\mathbf{x}) = \begin{cases} 1 & \forall \mathbf{x}\in\omega_i \\ 0 & \forall \mathbf{x}\notin\omega_i \end{cases}$ is the characteristic function of the integration subdomain. Note that the characteristic function is different from that in the derivation of the RT, which can be interpreted as that only the tracer mass in the subregion ω_i is considered for PRT_i.

Based on Eqs. (4) and (14), one can derive the following expression:

$$C_T^*(\mathbf{x}_0,t_0) = \iiint_{\omega_i} C(\mathbf{x},T)\,\mathrm{d}\mathbf{x} \tag{15}$$

Therefore, the adjoint variable $C_T^*(\mathbf{x}_0, t_0)$ denotes the mass of tracer in subregion ω_i at time T after the unit release at location $\mathbf{x}_0$ and time t_0. Based on Eqs. (7) and (15), RT equals

$$\overline{\theta}_{\omega_i}(\mathbf{x}_0, t_0) = \int_{t_0}^{\infty} C_T^*(\mathbf{x}_0, t_0)\mathrm{d}T. \tag{16}$$

Then, we can define the function $D(\mathbf{x}, t, \tau)$ as follows:

$$D(\mathbf{x}_0, t_0, \tau) = C_{t_0+\tau}^*(\mathbf{x}_0, t_0), \quad \tau > 0 \tag{17}$$

According to Eqs. (16) and (17), RT equals

$$\overline{\theta}_{\omega_i}(\mathbf{x}_0, t_0) = \int_{t_0}^{\infty} C_T^*(\mathbf{x}_0, t_0)\mathrm{d}T = \int_0^{\infty} D(\mathbf{x}_0, t_0, \tau)\mathrm{d}\tau. \tag{18}$$

According to Eq. (14), D should satisfy

$$\begin{cases} \dfrac{\partial D}{\partial t} - \dfrac{\partial D}{\partial \tau} + \mathbf{v}\cdot\nabla D + \nabla\cdot[\mathbf{K}\cdot\nabla D] = 0 \\ D(\mathbf{x}, t, 0) = \delta_{\omega_i}(\mathbf{x}) \end{cases}. \tag{19}$$

Assuming that $D(\mathbf{x}, t, \tau)$ decreases to 0 when τ trends to infinity, we can derive the RT equation by integrating Eq. (19) with respect to τ, i.e.,

$$\frac{\partial \overline{\theta}_{\omega_i}}{\partial t} + \delta_{\omega_i}(\mathbf{x}) + \mathbf{v}\cdot\nabla\overline{\theta}_{\omega_i} + \nabla\cdot\left[\mathbf{K}\cdot\nabla\overline{\theta}_{\omega_i}\right] = 0. \tag{20}$$

References

Blaise S, De Brye B, De Brauwere A, Deleersnijder E, Delhez ÉJM, Comblen R (2010) Capturing the residence time boundary layer—application to the Scheldt Estuary. Ocean Dyn 60(3):535–554

Blumberg AF, Mellor GL (1987) A description of a three-dimensional coastal ocean circulation model. Coast Estuar Sci 4:1–16

Bolin B, Rodhe H (1973) A note on the concepts of age distribution and transit time in natural reservoirs. Tellus 25(1):58–62

Chen DX (1992) Marine atlas of Bohai Sea, Yellow Sea, East China Sea: hydrology. China Ocean Press, Beijing **(in Chinese)**

de Brauwere A, De Brye B, Blaise S, Deleersnijder E (2011) Residence time, exposure time and connectivity in the Scheldt Estuary. J Mar Syst 84(3–4):85–95

Deleersnijder É, Campin JM, Delhez ÉJM (2001) The concept of age in marine modelling I. Theory and preliminary model results. J Mar Syst 28(2):29–267

Delhez ÉJM (2006) Transient residence and exposure times. Ocean Sci 2(1):1–9

Delhez ÉJM (2013) On the concept of exposure time. Cont Shelf Res 71: 27–36

Delhez ÉJM, Deleersnijder É (2002) The concept of age in marine modelling: II. Concentration distribution function in the English Channel and the North Sea. J Mar Syst 31(4):279–297

Delhez ÉJM, Deleersnijder É (2006) The boundary layer of the residence time field. Ocean Dyn 56(2):139–150

Delhez ÉJM, Heemink AW, Deleersnijder É (2004) Residence time in a semi-enclosed domain from the solution of an adjoint problem. Estuar Coast Shelf Sci 61(4):691–702

Ding WL (1992) Tides and tidal currents. In: Liu RY (ed) Ecology and living resources of Jiaozhou Bay. Science Press, Beijing, pp 39–57 **(in Chinese)**

Du J, Shen J (2016) Water residence time in Chesapeake Bay for 1980–2012. J Mar Syst 164:101–111

Editorial Board of Annals in China (1993) Jiaozhou Bay. In: Wang JL (ed) Annals of bays in China. Ocean Press, Beijing, pp 157–260. (in Chinese)

Feng S, Cheng RT, Pangen X (1986) On tide-induced Lagrangian residual current and residual transport: 1. Lagrangian residual current. Water Resour Res 22(12):1623–1634

Fraser MW, Kendrick GA (2017) Belowground stressors and long-term seagrass declines in a historically degraded seagrass ecosystem after improved water quality. Sci Rep 7(1):14469

Gong W, Shen J, Jia J (2008) The impact of human activities on the flushing properties of a semi-enclosed lagoon: Xiaohai, Hainan, China. Mar Environ Res 65(1):62–76

Gong W, Shen J, Cho KH, Wang HV (2009) A numerical model study of barotropic subtidal water exchange between estuary and subestuaries (tributaries) in the Chesapeake Bay during northeaster events. Ocean Model 26(3–4):170–189

Jeyar M, Chaabelasri E, Salhi N, Borthwick AG, Elmahi I (2017) Numerical modelling of transport time scales within Nador lagoon (Morocco). World J Model Simul 13(2):113–122

Jickells TD (1998) Nutrient biogeochemistry of the coastal zone. Science 281(5374):217–221

Lillebø AI, Neto JM, Martins I, Verdelhos T, Leston S, Cardoso PG et al (2005) Management of a shallow temperate estuary to control eutrophication: the effect of hydrodynamics on the system's nutrient loading. Estuar Coast Shelf Sci 65(4):697–707

Lin L, Liu Z (2019) TVDal: total variation diminishing scheme with alternating limiters to balance numerical compression and diffusion. Ocean Model 134:42–50

Lin L, Liu Z, Xie L, Gao H, Cai Z, Chen Z, Zhao J (2015) Dynamics governing the response of tidal current along the mouth of Jiaozhou Bay to land reclamation. J Geophys Res-Oceans 120(4):2958–2972

Lin L, Liu D, Liu Z, Gao H (2016) Impact of land reclamation on marine hydrodynamic and ecological environment. Haiyang Xuebao 38(8): 1–11 **(in Chinese with English abstract)**

Liu Z, Wei H, Liu G, Zhang J (2004) Simulation of water exchange in Jiaozhou Bay by average residence time approach. Estuar Coast Shelf Sci 61(1):25–35

Liu G, Liu Z, Gao H, Gao Z, Feng S (2012a) Simulation of the Lagrangian tide-induced residual velocity in a tide-dominated coastal system: a case study of Jiaozhou Bay, China. Ocean Dyn 62(10–12):1443–1456

Liu Z, Wang H, Guo X, Wang Q, Gao H (2012b) The age of Yellow River water in the Bohai Sea. J Geophys Res-Oceans 117:C11

Liu Z, Lin L, Xie L, Gao H (2016) Partially implicit finite difference scheme for calculating dynamic pressure in a terrain-following coordinate non-hydrostatic ocean model. Ocean Model 106:44–57

Luan WX, Dong A (2002) The fundamental programs of marine functional division of China. Hum Geogr 17(3):93–95 (in Chinese with English abstract)

Lucas LV, Thompson JK, Brown LR (2009) Why are diverse relationships observed between phytoplankton biomass and transport time? Limnol Oceanogr 54(1):381–390

Luff R, Pohlmann T (1995) Calculation of water exchange times in the ICES-boxes with a Eulerian dispersion model using a half-life time approach. Deutsche Hydrografische Zeitschrift 47(4):287–299

Lv X, Zhao C, Xia C, Qiao F (2010) Numerical study of water exchange in the Jiaozhou bay and the tidal residual currents near the bay mouth. Acta Oceanol Sin 32(2):20–30 **(in Chinese with English abstract)**

Meyers SD, Moss AJ, Luther ME (2017) Changes in residence time due to large-scale infrastructure in a coastal plain estuary. J Coast Res 33(4):815–828

Monsen NE, Cloern JE, Lucas LV, Monismith SG (2002) A comment on the use of flushing time, residence time, and age as transport time scales. Limnol Oceanogr 47(5):1545–1553

Mouchet A, Cornaton F, Deleersnijder E, Delhez ÉJ (2016) Partial ages: diagnosing transport processes by means of multiple clocks. Ocean Dyn 66(3):367–386

Oey L (2005) A wetting and drying scheme for POM. Ocean Model 9(2): 133–150

Oey L (2006) An OGCM with movable land–sea boundaries. Ocean Model 13(2):176–195

Olsen YS, Fraser MW, Martin BC, Pomeroy A, Lowe R, Pedersen O, Kendrick GA (2018) In situ oxygen dynamics in rhizomes of the seagrass Posidonia sinuosa: impact of light, water column oxygen, current speed and wave velocity. Mar Ecol Prog Ser 590:67–77

Prandle D (1984) A modelling study of the mixing of 137Cs in the seas of the European continental shelf. Philos Trans R Soc Lond A 310(1513):407–436

Qingdao Marine Environment Bulletin, 2017. http://ocean.qingdao.gov.cn

Ranjbar MH, Zaker NH (2017) Numerical modeling of general circulation, thermohaline structure, and residence time in Gorgan Bay, Iran. Ocean Dyn 68:1), 1–1),12

Shi J, Li G, Wang P (2011) Anthropogenic influences on the tidal prism and water exchanges in Jiaozhou Bay, Qingdao, China. J Coast Res 27(1):57–72

Silverman BW (1986) Density estimation for statistics and data analysis, vol 175. Chapman & Hall, London

Spivakovskaya D, Heemink AW, Deleersnijder E (2007) Lagrangian modelling of multi-dimensional advection-diffusion with space-varying diffusivities: theory and idealized test cases. Ocean Dyn 57(3):189–203

Sun J, Lin B, Li K, Jiang G (2014) A modelling study of residence time and exposure time in the Pearl River Estuary, China. J Hydro Environ Res 8(3):281–291

Takeoka H (1984) Fundamental concepts of exchange and transport time scales in a coastal sea. Cont Shelf Res 3(3):311–326

Van Sebille E, Griffies SM, Abernathey R, Adams TP, Berloff P, Biastoch A et al (2018) Lagrangian ocean analysis: fundamentals and practices. Ocean Model 121:49–75

Wang C, Zhang XQ, Sun YL (2009) Numerical simulation of water exchange characteristics of the Jiaozhou Bay based on a three-dimensional Lagrangian model. China Ocean Eng 23(2):277–290

Yuan D, Lin B, Falconer RA (2007) A modelling study of residence time in a macro-tidal estuary. Estuar Coast Shelf Sci 71(3–4):401–411

Zheng PY (1994) The marine function and functional division of Jiaozhou Bay. Coast Eng 13(4):63–69 **(in Chinese with English abstract)**